Acta Geotechnica
https://doi.org/10.1007/s11440-024-02270-7

RESEARCH PAPER

Shear strength recovery of sand with self-healing polymeric capsules

Rui Qi[1] · Ke Chen[1] · Hongjie Lin[2] · Antonios Kanellopoulos[3] · Liu Deyun[4] · Anthony Kwan Leung[5] · Sérgio D. N. Lourenço[1]

Received: 13 April 2023 / Accepted: 16 January 2024

Abstract
Self-healing approaches are increasingly being explored in various fields as a potential method to recover damaged material properties. By self-recovering without external intervention, self-healing techniques emerge as a potential solution to arrest or prevent the development of large strains problems in soils (e.g., landslides) and other ground effects that influence the serviceability of structures (e.g., differential settlement). In this study, a microcapsule-based self-healing sand was developed, and its performance during mixing and compaction, shearing, and recovery of shear strength was demonstrated. The cargo used for sand improvement, a hardening oil, tung oil, was encapsulated in calcium alginate capsules by the ionic gelation method. The surface properties, internal structure, thermal stability and molecular structure of the capsules were evaluated by advanced material characterization techniques. The survivability of capsules during mixing and compaction was assessed by measuring the content of tung oil released into the sand, while their influence on sand shear strength and its recovery was assessed with shear box tests. The results showed that the capsules could rupture due to movement of the sand particles, releasing the tung oil cargo, leading to its hardening and minimizing its strain-softening response and enhancing up to 76% of the sand shear strength (at a normal stress of 10 kPa and capsules content of 4%). This study demonstrates the potential of a capsules-based self-healing system to provide 'smart' autonomous soil strength recovery and thus with potential to actively control the large strain behavior of soils.

Keywords Microcapsules · Sand · Self-healing · Shear strength

1 Introduction

Recent research on self-healing materials inspired the possible application of self-healing methods in the recovery of damaged or weakened soil. For instance, as a city with a dense urban development near hillsides, Hong Kong is vulnerable to natural terrain landslides [23]. Slope stabilization makes use of conventional methods including earth retaining structures and drainage. Recently, microbial-induced calcite mineralization has been proposed to mitigate landslide risks, with field data revealing slower displacement rates for the bio-stabilized zone compared to non-stabilized areas [36]. Compared to the conventional methods, the microcapsules can be activated to enhance slope stability when needed, thereby contributing to their safety and stability.

Self-healing refers to the ability of a material to recover from degradation or damage through adaptation and response to external stimuli without human intervention [6]. They can fully or partially recover a property that has

✉ Sérgio D. N. Lourenço
lourenco@hku.hk

1 Department of Civil Engineering, The University of Hong Kong, Pok Fu Lam, Hong Kong SAR, China

2 School of Civil Engineering, Sun Yat-Sen University, Guangzhou, China

3 School of Physics, Engineering and Computer Science, Centre for Engineering Research, University of Hertfordshire, Hatfield, UK

4 Department of Civil and Environmental Engineering, Polytechnic University of Hong Kong, Hung Hom, Hong Kong SAR, China

5 Department of Civil and Environmental Engineering, Hong Kong University of Science and Technology, Clear Water Bay, Hong Kong SAR, China

Published online: 23 March 2024

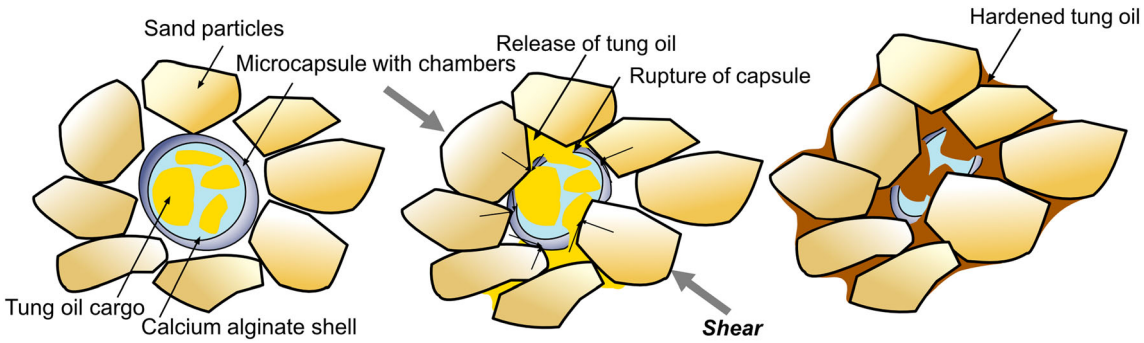

Fig. 1 Conceptual diagram of soil mechanical properties recovery by polymeric capsules: shearing with sand particles and rupture of capsules, release of tung oil cargo, its hardening and bonding of sand particles

been affected by in-service actions [4]. In cement-based composites, self-repairing technologies include microorganisms [13], liquid core fibers [14], and microcapsules [15]. Among these approaches, microcapsule-based self-healing has the benefits that: (i) does not lead to the development of major discontinuities in the matrix as for example vascular networks do [34] and, (ii) does not rely on the availability of nutrients as is the case on biological healing approaches [35].

The microencapsulation healing mechanism is based on the fact that when the developing crack front hits the outer shell of the microcapsules, this will rupture, subsequently leading to the release of encapsulated healing agents. The healing compounds will then undergo a series of chemical reactions, which depend on their nature and type, and will lead to the healing of the formed cracks, and the recovery of material properties. In concrete, microcapsules with sodium silicate cargo and polymer shell were synthesized and applied to cement specimens. The results showed the reduced sorptivity of cracked specimens over a 28-day healing period [15]. In cement mortars incorporating microcapsules, the crack mouth healing reached almost 100% and the healing in terms of measured crack depth and sorptivity coefficient found to be to a maximum of 70% and 54%, respectively [21]. In pavements, calcium-alginate microcapsules containing sunflower oil were mixed with asphalt mastic, healing their cracks and thus were expected to develop sustainable long-life asphalt pavements [1, 39].

The use of microcapsules in ground applications has been limited to cemented soils. Microcapsules with epoxy resin cargo were applied to cemented coral sand, with the compressive strength of the pre-damaged specimen increased by approximately 85% with 3% of microcapsules by weight. Furthermore, the potential of microcapsules as a self-healing agent for cemented soil in cutoff walls has also been demonstrated [7] with the results showing that the microcapsule-containing post-healing specimens regained 44% of their initial compressive strength after damage and also showed reduced hydraulic conductivity. Although these studies demonstrate the potential of microcapsules in ground applications (i.e., cutoff walls), the cemented matrix of the tested soils results in a self-healing mechanism similar to cementitious materials. The suitability of microcapsules for self-healing applications in unbound granular materials (without any form of bonding or cementation) remains an unexplored area.

The cargo release mechanism in granular materials will differ from cementitious materials. In cementitious materials, the self-healing effect relies on the rupture of microcapsules and the subsequent release of their cargo by intersecting cracks. Then there is a chemical reaction between the cargo and the surrounding matrix which leads to healing of cracks. In this study, we hypothesize that the microcapsules loaded with a healing agent rupture due to the movement of soil particles' (under axial or volumetric strains). The rupture of microcapsules and the release of the cargo is followed by hardening and physical bonding of particles to create a cement-like supported soil matrix and hence leading to the enhancement of the soil mechanical strength (Fig. 1). Compared to conventional ground improvement methods, capsules possess the advantage of being smart materials. They respond to soil shearing and automatically reinforce weak areas. This self-healing capability reduces the need for continuous monitoring and mitigation works. In addition, capsules can be tailored to minimize changes to other soil properties and environmental disruption.

The main challenges to be addressed in this study concern the interaction of capsules with soil particles, how they release their cargo, and how this cargo contributes to increased shear strength. Given the limited prior research in capsule applications in granular materials, this study serves as a feasibility assessment before embarking on a broader experimental program. This study investigates for the first time the performance of unbound granular materials with a microcapsule-based self-healing mixture. Tung oil was used as the healing agent as it could polymerize when exposed to air, forming a hard film [40]. Capsules with the

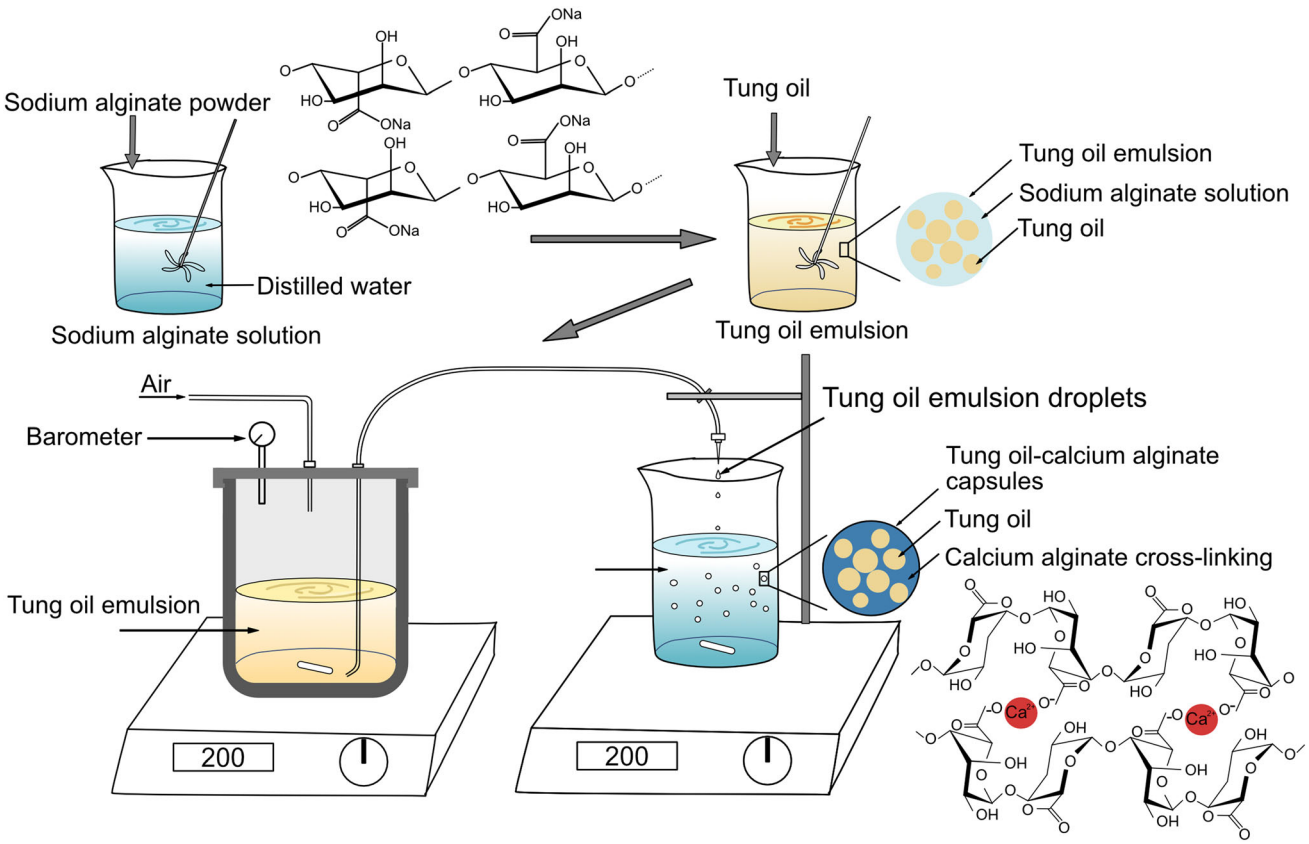

Fig. 2 Encapsulation process of tung oil-calcium alginate capsules

healing agent (tung oil) were synthesized at variable sizes and cargo loadings (i.e., cargo percentage by mass). The influence of capsules on the shear strength of a clean sand was investigated by shear box tests with their self-healing effectiveness assessed in terms of the shear strength increase and released cargo percentage. To assess the self-healing efficiency, testing was conducted in fresh tung oil (liquid state) and aged tung oil (solid state). The capsules and granular material mixtures were prepared in advance by mixing and compaction, with their survivability assessed by measuring the percentage of cargo release. The maximum and minimum dry density were also measured.

2 Materials and methods

2.1 Materials

Tung oil (Jogel Co., China) was used as the healing cargo. Tung oil is a drying oil obtained by pressing seeds from the nut of the Tung tree, and it is non-toxic and relatively inexpensive [18, 25]. An ecotoxicity assessment revealed minimal impact on soil microorganisms by tung oil [25]. Fresh tung oil is made of unsaturated glycerides of long chain fatty acids, with a transparent color and good liquidity. During polymerization, the cleavage of the carbon–carbon chain leads to the cross linking of the tung oil's molecules forming a solid film [24]. Past research showed that tung oil can be encapsulated and has proved to heal artificial scratches in epoxy coatings [32]. Moreover, tung oil mixed with completely decomposed granite showed an increase in aggregate tensile strength, from 632 to 2641 kPa [24].

Sodium alginate ($NaC_6H_7O_6$) and calcium chloride ($CaCl_2$) were used to form the shell (Sigma-Aldrich, USA). Alginate is an unbranched block copolymer composed of the two glycan monomers β-d-mannuronic acid and α-l-guluronic acid [3]. Sodium alginate is non-toxic, biodegradable and derives from naturally occurring polysaccharides [20, 27], which was used to form the shell. These characteristics make them an attractive candidate material for application in soils. The mechanism of the capsules shell formation is based on the cross-linking of sodium alginate and calcium cations [9, 26, 29].

Sieved clean silica sand was selected as the host granular material (Fantasy Quartz Sand Supply Company, China). It is composed of silica, with the main constituent being silicon dioxide (SiO_2). The sand particle size distribution varied from 0.6 mm to 1.18 mm (a comparison with the capsules size distribution is shown in Fig. 3a, with a

ratio of medium sand size relative to the medium capsule size of 0.66). The particle shape parameters of the sand were measured, with an aspect ratio of 0.72, indicating an angular shape.

2.2 Tung oil-calcium alginate capsules synthesis

Tung oil was encapsulated in calcium alginate with the ionic gelation method. This method is based on the formation of an emulsion of tung oil and sodium alginate solution and the formation of the capsules' shell by crosslinking of sodium alginate in a $CaCl_2$ solution.

The encapsulation process was as follows (Fig. 2): (1) *Formation of tung oil and sodium alginate emulsion:* 1.5 g sodium alginate was dissolved in 100 g distilled water with an overhead high speed steerer (IKA RW20 digital, Germany) at 200 rotations/min, and 20 g tung oil was slowly added to the sodium alginate solution, at a stirring speed of 800 rotations/min until a stable emulsion was formed; (2) *Formation of capsules' shell:* As shown in Fig. 2, the tung oil and sodium alginate emulsion was dripped into a $CaCl_2$ solution (1.0 M) at room temperature, by means of a syringe with inner diameter 0.26 mm under an air pressure of 10 kPa. The shell formed when the tung oil and sodium alginate emulsion was introduced into a $CaCl_2$ solution prepared by dissolving the 59.9 $CaCl_2$ powder in 500 mL distilled water and remained in the $CaCl_2$ bath for 24 h. Sodium alginate gelation took place as divalent cations (Ca^{2+}) interacted ionically with blocks of guluronic acid residues of sodium alginate, resulting in the formation of a three-dimensional network, which was the calcium alginate [17]. *(3) Filtration:* Following this, the capsules were filtered with a vacuum pump (LongerPump WT3000-1JB, China), rinsed with distilled water, and dried at ambient temperature ($\sim$ 25 °C) for 24 h. With the evaporation of water, drying leads to shrinkage, increasing the tung oil loading in the capsules.

2.3 Characterization of capsules

The morphology, inner structure, and physicochemical properties of the capsules were evaluated. The surface morphology and inner structure of the capsules were observed by scanning electron microscopy (SEM) (Hitachi S3400N VP SEM). The capsules were coated with an AuPd alloy film to conduct electricity and scanned at a voltage of 5 kV. Element mapping of the calcium alginate-tung oil composite was conducted by energy dispersive spectroscopy (EDS) with the same settings. The capsules size distribution were characterized by a dynamic image analyser QicPic™ (Sympatec GmbH, Clausthal-Zellerfeld, Germany). Cumulative distributions of particle size were generated by analyzing the two-dimensional (2D) profiles of the particles falling by gravity. 2D binary images of the particles were taken during their falling at a frame rate of 300 Hz. The resolution of the lens in the camera was 10 μm. Physicochemical assays included thermal gravimetric analysis (PerkinElmer TGA 4000) ranging from 25 to 950 °C with a heating rate of 20 °C/min in N_2 flow (20 ml/min) and, Fourier transform infrared analysis (PerkinElmer Frontier IR single-range spectrometer) in the range of 4000–400 cm^{-1}.

2.4 Capsules survivability during sample preparation

The survivability of capsules during sample preparation, i.e., mixing and compaction was assessed by measuring the amount of tung oil that leaked into the sand. A lower leaking amount indicated higher capsules survivability. Samples containing the increasing capsules content were prepared. The capsules content used for this study was 4%, 8%, and 12% of mass ratio, which correspond to a tung oil content of 2.8%, 5.6%, and 8.4%.

The amount of tung oil that leaked into the sand was measured by removing the capsules and recording the mass change of sand samples before and after heating. The capsules were collected manually given that they were visually distinguishable. The melting temperature of quartz is substantially higher at approximately 1700 °C, while tung oil decomposes at temperatures below 600 °C [19]. Thus, the sand samples were heated to 600 °C in a furnace (Protherm furnaces ECO110, Germany), and their mass was measured before and after heating using a semi-micro-analytical balance (Sartorius SECURA225D-1S, Germany). There could be other residual components within the sand that may decompose during the heating process. Therefore, the mass was calibrated as the mass changes before and after heating of clean silica sand. The content of the released tung oil in the sand w_{tc} was calculated using Eq. (1):

$$w_{tc} = \frac{\text{Released tung oil amount}}{\text{Mass of soil sample}} \times 100\% \quad (1)$$

As the tung oil content of capsules was 70% (from the TGA results), the amount of released tung oil accounts for the percentage of the total tung oil content of the capsule w_{rp} and was calculated following Eq. 2:

$$w_{rp} = \frac{\text{Released tung oil amount}}{\text{Mass of microcapsules} \times 70\%} \times 100\% \quad (2)$$

The mixing procedure was based on mixing 2 kg of sand with the three different capsules content (4%, 8%, and 12%) using an overhead stirrer (IKA RW20 digital, Germany) at 200 rotations/min. Mixing lasted until capsules were evenly distributed in the sand (assessed visually). Due

to the large amount of sand, random sub-samples were then collected, and the released tung oil amount was measured.

The microcapsule's survivability was also assessed after compaction following the Proctor compaction test (detailed in Sect. 2.5). Samples were then collected from the top, middle, and bottom of the compacted sample with the released tung oil amount calculated with Eq. (1).

2.5 Maximum and minimum dry density

The minimum and maximum dry density of sand-capsules mixtures with different capsules content was measured. Standard Proctor compaction tests [37] were carried out to determine the maximum dry density of the sand-capsules mixtures, by placing the mixtures in a standard 0.95-L volume cylindrical mold in 3 layers. Each layer was compacted by applying 25 blows with a 2.5 kg rammer falling from an elevation of 30.48 cm. The test was repeated for each capsule's content, to obtain the maximum dry density. The minimum dry density of the sand-capsules mixture was measured with the cylinder method [2]. A 1000 g sand-capsules mixture was placed in a 2000 mL graduated cylinder. The top of the cylinder was covered with a plate, and the sample is turned upside down, then steadily rotated back upright at a constant rate, taking approximately 30–60 s to reach vertical [8]. This procedure allowed the sand-capsules mixture to reach its maximum volume. The volume of sand was then measured using the gradations on the graduated cylinder, and the density was calculated.

2.6 Recovery of sand shear strength with capsules

At first, the impact of the capsules with fresh tung oil on the sand shear strength was measured by direct shear tests. The preparation process for the direct shear samples is as follows. (1) Mixing of sand and capsules: the capsules were mixed into the sand according to the predetermined capsule content levels (4%, 8%, and 12%) thoroughly to achieve a uniform distribution. (2) Determination of sample mass: the relative density was the same for all samples (70%). The amount of the sand-capsules mixture required for the shear box samples was calculated based on the data for maximum and minimum dry densities. For the clean sand and sand mixed with 4%, 8%, and 12% capsule content, this corresponded to a mass of 478 g, 461 g, 442 g, and 437 g, respectively. (3) Layering and compaction: the sand and sand-capsules mixture were transferred and compacted into a shear box with dimensions of 3 × 10 × 10 cm with three layers. A uniform pressure was applied to achieve the desired relative density. Given that the measured specific gravity of capsules was 0.98, the void ratio was calculated, and the bulk density, relative density, and void ratio of the prepared samples are summarized in Table 1.

The sand-capsules mixtures were sheared in a dry condition under normal stresses of 10 kPa, 30 kPa, 50 kPa, and 100 kPa and a shearing rate of 1 mm/min. To analyze the direct shear test, the mobilized friction angle (ϕ_d) and dilation angle in direct shear (ψ) was calculated with the equation next [5, 12, 31]:

$$\tan \phi_d = \tau / \sigma \tag{3}$$

$$\tan \psi = \delta_v / \delta_h \tag{4}$$

where τ = shear stresses, σ = normal stresses, δ_v = incremental vertical displacement, and δ_h = incremental horizontal displacement during shear.

In addition, the capsules' potential to fracture and subsequently release their cargo was assessed during the shearing process. After shearing, sub-samples were collected from the top, bottom, and middle of the shear box. The top and bottom sub-samples represent those in the compacted areas, whereas the middle one refers to the sample at the shearing zone. The released cargo amount in these sub-samples was measured with the method detailed in Sect. 2.4. The collected samples were observed with SEM.

The ability of aged tung oil capsules to recover sand shear strength was also assessed by shear box tests in dry samples. Shearing was conducted in three stages: (1) first shearing to force the rupture and release of cargo; (2) tung oil hardening and, (3) second shearing of the healed samples. Procedures were as follows: a total of 478 g of sand only, sand with blank alginate capsules (both are control groups) and sand with tung oil Ca-alginate capsules were mixed at 4% capsules content and sheared to a horizontal strain of 2% at normal stresses of 10, 30, 50, and 100 kPa, after which shearing was stopped and the samples were unloaded (both the shear and vertical components). The exact same loading sequences were applied to all the sand samples and the blank capsules group. Healing

Table 1 Bulk density, relative density, and void ratio of sand and sand mixed with 4%, 8% and 12% tung oil-calcium alginate capsules

	Bulk density	Relative density	Void ratio
Sand	1.45	0.7	0.83
Sand mixed with 4% capsules	1.4	0.7	0.78
Sand mixed with 8% capsules	1.34	0.7	0.76
Sand mixed with 12% capsules	1.32	0.7	0.69

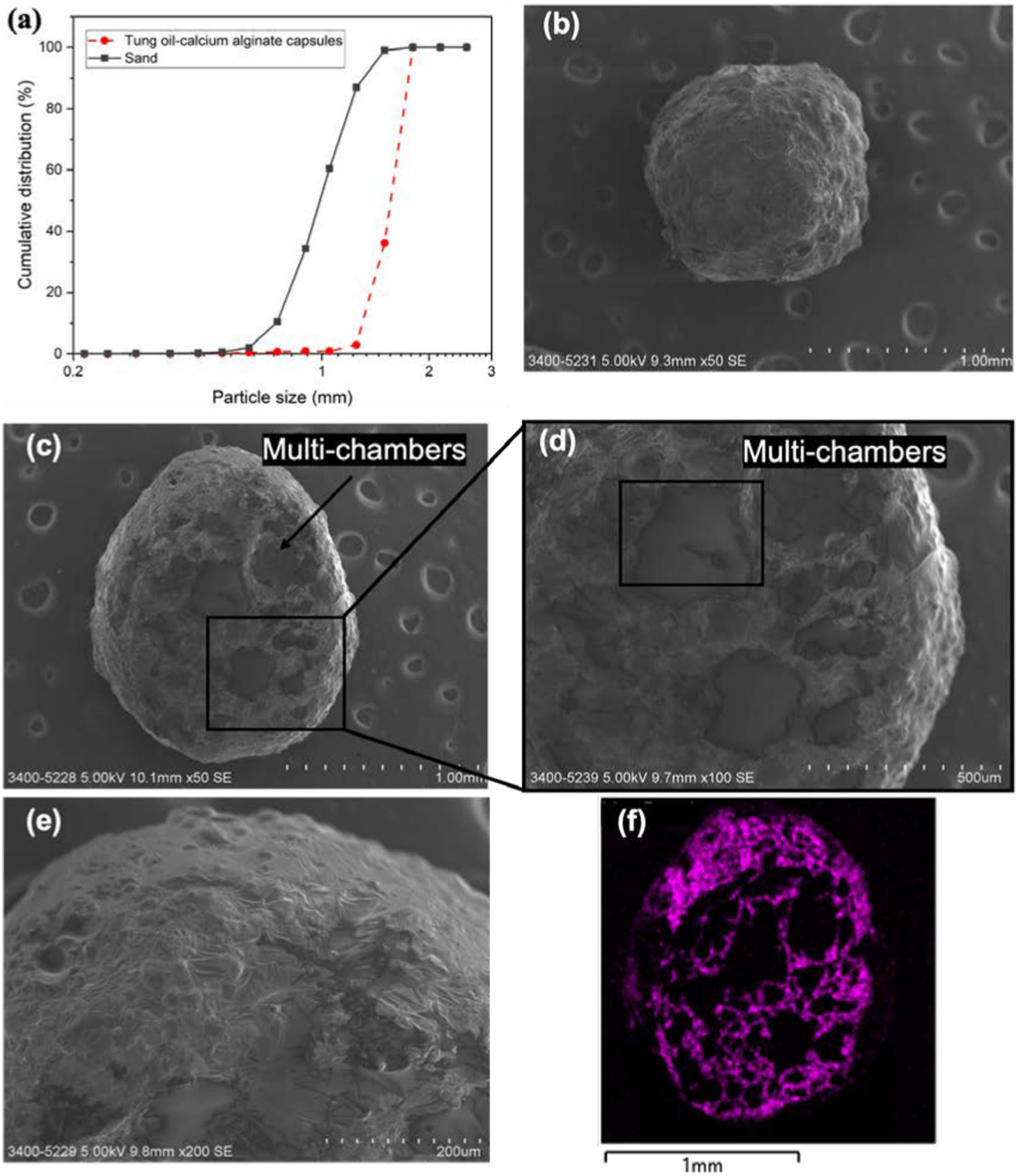

Fig. 3 Physical properties of tung oil-calcium alginate capsules: **a** silica sand and capsules particle size distribution; **b** SEM photomicrographs of capsules (50 ×); **c** SEM photomicrographs of a cross-Sect. (50 ×) and **d** (100 ×); **e** surface morphology by SEM (200 ×); **f** Elemental mapping of Ca by Energy Dispersive Spectroscopy

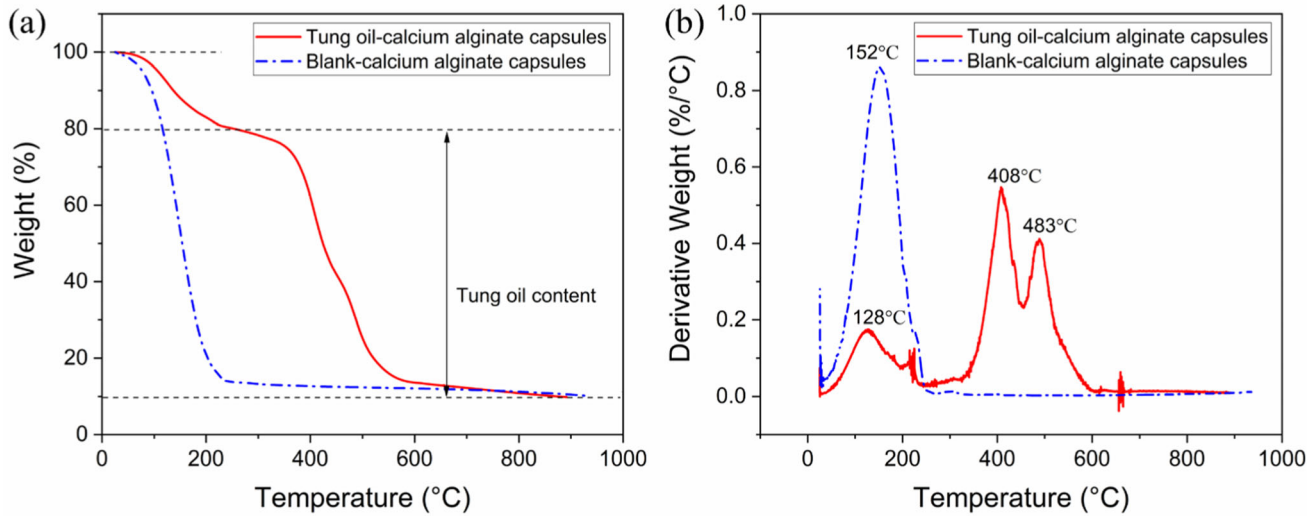

Fig. 4 TGA thermograms of tung oil-calcium alginate capsules and blank-calcium alginate capsules: **a** Weight loss curves; **b** Derivative thermogravimetric curves

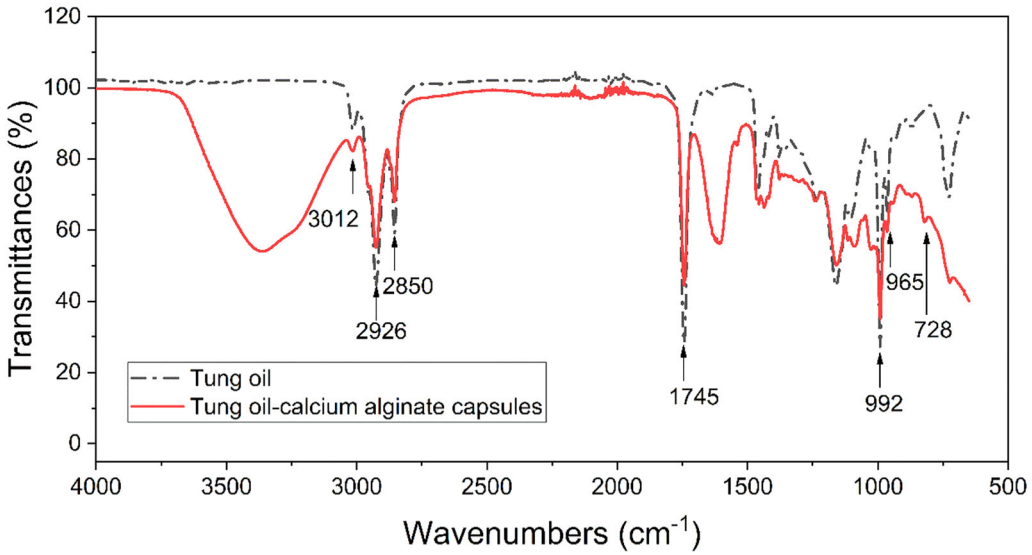

Fig. 5 Fourier transform infrared analysis of tung oil-calcium alginate capsules and tung oil

performances were examined by comparing the shear strength behavior of sand only, to sand with capsules after the shear strength recovery.

Blank capsules refer to capsules without a tung oil core and consist solely of calcium alginate. They are similar in size, shape, and stiffness to the tung oil-calcium alginate capsules. The blank capsules were used as a control condition to isolate and evaluate the impact of the tung oil cargo on the soil's shear strength. In this study, the samples were unloaded and placed in an incubator for the strength recovery process as the hardening of tung oil requires exposure to oxygen. According to preliminary data, heating accelerated the hardening of tung oil, by placing sand-capsules samples for 48 h at 60 °C. Comparable shear strength gains can be achieved by placing the samples at a relative humidity of 40% for 14 days under a standard reference temperature (25 °C). Therefore, to expedite the testing program, samples were placed in an incubator (60 °C , relative humidity 40%) for 48 h for accelerated tung oil hardening and to allow shear strength recovery. In

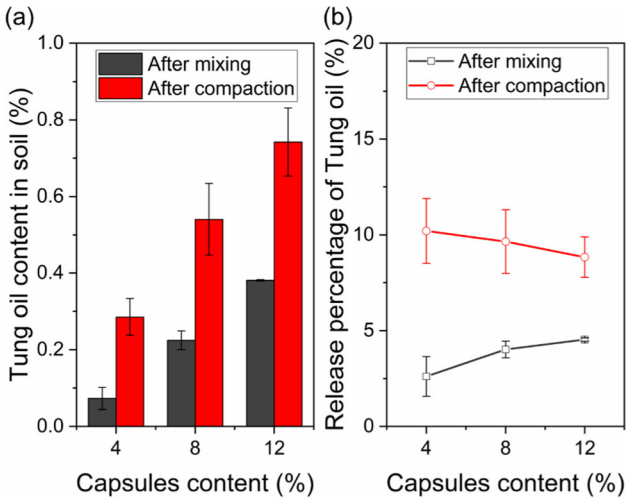

Fig. 6 Cargo release during mixing and compaction process of silica sand and tung oil capsules. **a** released tung oil content in sand; **b** released tung oil percentage from capsules

Table 2 Minimum and maximum dry density of sand and sand mixed with 4%, 8% and 12% tung oil-calcium alginate capsules

Capsules' density	Minimum dry density (kg/L)	Maximum dry density (kg/L)
0%	1.29 ± 0.002	1.56 ± 0.006
4%	1.21 ± 0.003	1.53 ± 0.008
8%	1.14 ± 0.003	1.48 ± 0.007
12%	1.13 ± 0.002	1.46 ± 0.001

addition, samples after healing were collected and observed by SEM.

3 Results and discussion

3.1 Characterization of capsules

3.1.1 Size characterization

The physical properties of the capsules were characterized and shown in Fig. 3. Figure 3a shows the capsules size (diameter) distribution curve. The majority (approximately 95%) of the capsules were distributed between 1.2 and 1.7 mm. The average particle size of the capsules was 1.5 mm. The size of these capsules is primarily determined by the particle size of the emulsion used during the encapsulation process. As a result, there is no upper bound size for this type of capsule. In practice, the most produced capsule sizes within this category typically fall within the range of 0.5 mm to 2 mm in diameter. The host material, silica sand, had a particle size distribution in the range of 0.6–1.18 mm. Chen et al. assessed the retention of capsules under seepage water in order to define a constriction size retention criterion [10]. These capsules ranges ensure that, according to the constriction size retention criterion of calcium alginate capsules, more than 95% of the capsules will not be lost when subject to water seepage, guaranteeing the potential self-healing efficiency triggered by capsules in granular materials. Also, the capsules will not be cracked during mixing even though their particle size ranges are larger, which will be proved later. Figure 3b, c shows the shape and surface features of the dried capsules. The capsules had a relatively spherical shape with the dried capsules showing a rough surface which is assumed to be attributed to the high calcium ion concentration [28]. Figure 3c, d is the SEM image of the capsules cross-section, showing a multi-chamber internal structure. The size and shape of these small cells were possibly controlled by the size of the tung oil droplets in the emulsion [38]. Figure 3f shows the calcium element mapping by EDS revealing that the calcium alginate forms a skeleton that supports the chambers with tung oil. For capsules ruptured mechanically, as there are multiple chambers, the breakage of capsules will lead to partial leakage of the cargo.

3.1.2 TGA

The proportion of encapsulated cargo, the decomposition of the capsules, and the thermal stability of capsules were evaluated by thermogravimetric analysis. Figure 4 shows the thermogravimetric analysis curves of blank capsules and capsules with tung oil cargo. For capsules encapsulated with tung oil cargo, the first stage of mass loss in the range of 0–250 °C represents dehydration (25–100 °C), decomposition of calcium alginate and volatilization of tung oil (170–250 °C). The second stage occured between 250–600 °C, corresponding to the decomposition of tung oil. For blank capsules, the decomposition process only included dehydration and calcium alginate decomposition. The tung oil content was estimated at approximately 70% using the blank capsules as a reference. Figure 4b shows the endothermic curve of blank capsules and capsules with tung oil. The first heat absorption peak of the tung oil capsules was 128 °C, which was lower than that of blank capsules (150 °C) because of the heat absorption by the volatilization of tung oil. Another two heat absorption peaks at 408 °C and 483 °C were detected, indicating the decomposition of tung oil. Similar results have also been reported in the literature [18]. In addition, both results

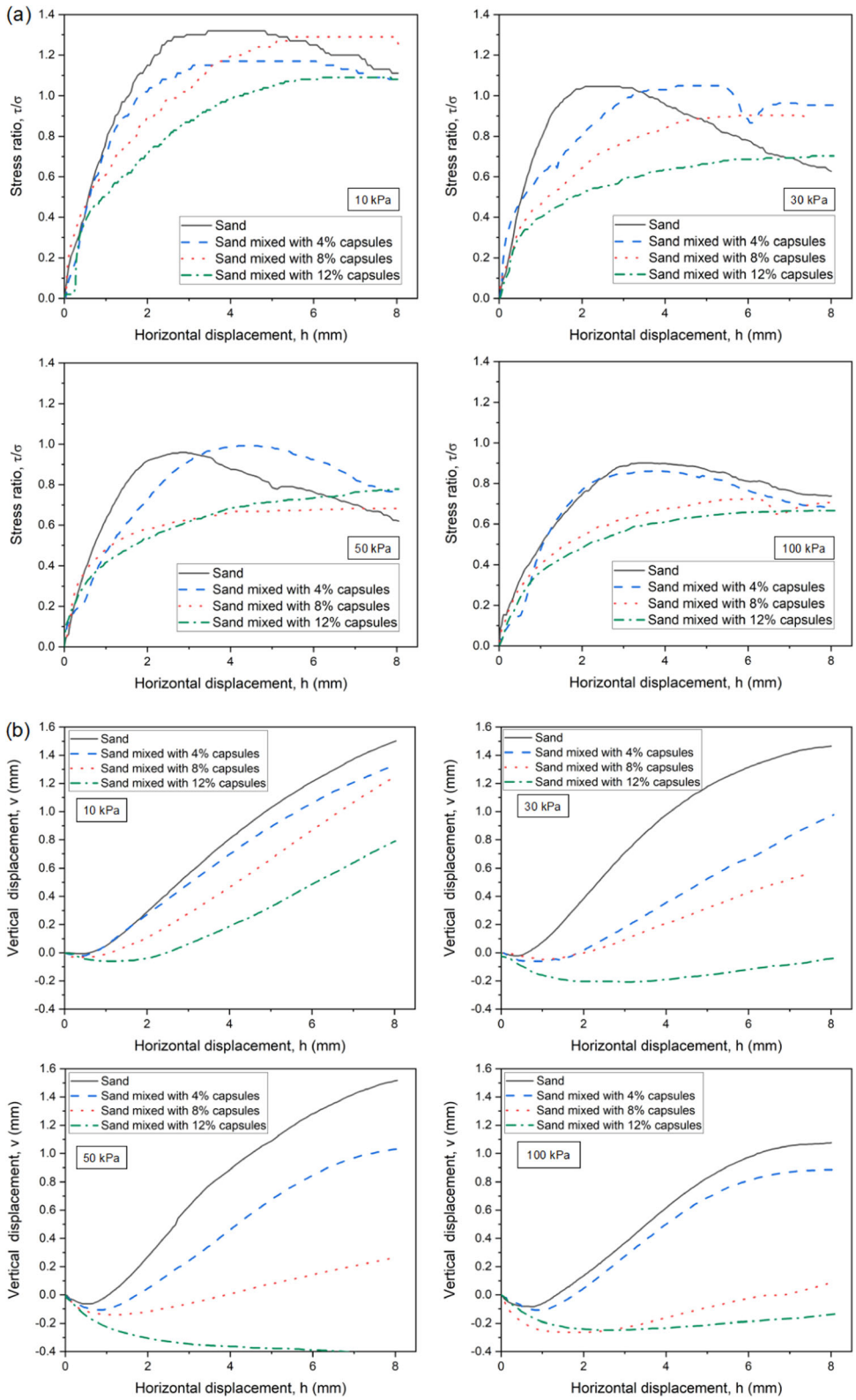

Fig. 7 The shear response of silica sand mixed with tung oil-calcium alginate capsules: **a** stress ratio (τ/σ) versus horizontal displacement (h); **b** vertical displacement (v) versus horizontal displacement (h); **c** dilatancy ($\delta v/\delta h$) versus horizontal displacement (h)

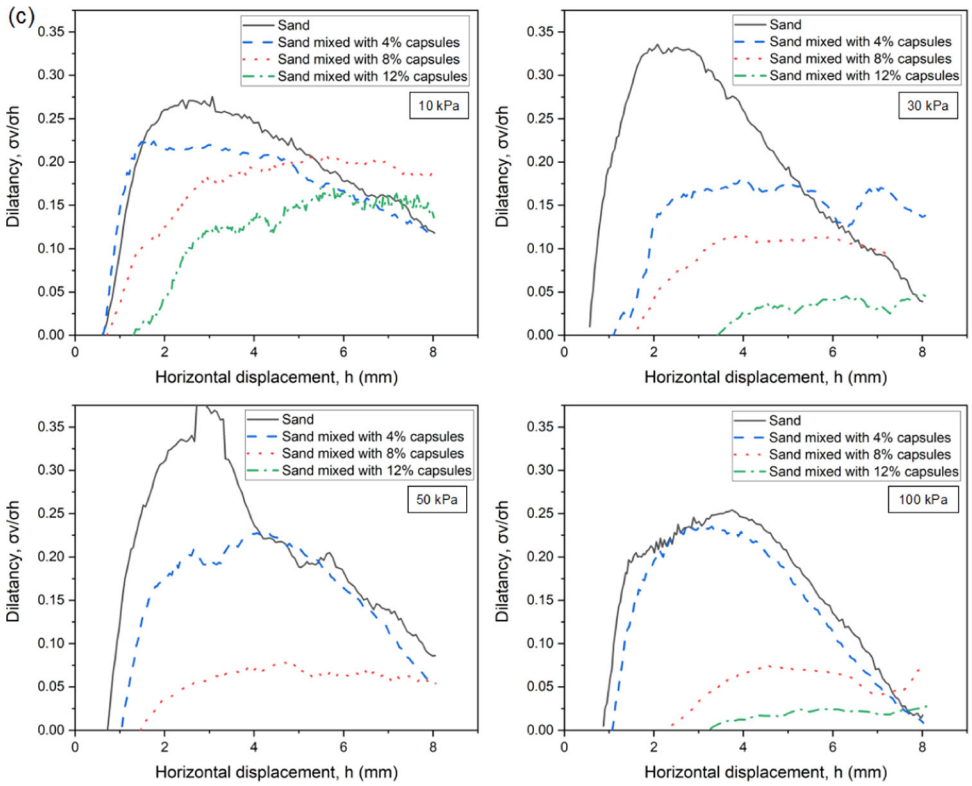

Fig. 7 continued

suggest the capsules are stable for a temperature range of 10–40 °C, which matches the seasonal soil temperature change in Hong Kong [11].

3.1.3 FTIR

FTIR was used to assess the presence of characteristic groups in the capsules. Figure 5 shows the FTIR results of tung oil and capsules with tung oil cargo. The peaks at 2926 cm^{-1} and 2850 cm^{-1} showed the symmetric and asymmetric C–H stretching vibration of the methyl group (α-eleostearic acid); the peak at 1745 cm^{-1} confirmed the presence of hydrogen-bonded carboxyl groups; the absorptions of 992 cm^{-1} and 965 cm^{-1} indicated C = C stretching of the conjugate alkenyl groups of α-eleostearic acid; and the peak at 728 cm^{-1} represented C–H bending vibration of the cis-configuration of the alkenyl group [33]. These characteristic groups indicated the encapsulation of tung oil.

3.2 Capsules' survivability during sample preparation

Sufficient capsules' mechanical strength is necessary to ensure their survival during mixing and compaction with sand. The release amount of cargo during mixing and compaction was measured and shown in Fig. 6. On average, tung oil content in the sand after mixing was 0.2% (Fig. 6a). This corresponds to approximately 4% cargo release (Fig. 6b) from the capsules in the mixing process with the sand, indicating that 96% of the cargo remained in the capsules. After compaction, the average tung oil content in sand increased to 0.5%, corresponding to approximately 10% of cargo leaking out (90% of the cargo remained in capsules). With the increase of capsules content from 4 to 12%, the content of tung oil in sand after mixing increased from 0.07% to 0.38%, suggesting a decreasing survival rate from 97.4% (4% capsules content) to 95.5% (12% capsules content). Similar results were

observed for the effect of the capsules content on the release of cargo and capsules survival, i.e. decreasing survival rate for increasing capsules content. As the survivability was measured when the soil reached the maximum soil density, it provided insight into the capsule's survival under extreme conditions and served as a reference point. In engineering practice, when capsules are mixed with the soil and then compacted, survivability is expected to be comparable to the values observed. The limited release of tung oil can be explained by the multi-chambers structure of capsules, which lead to limited cargo release and enhance the survivability of capsules. Another factor that could have also contributed to the limited release is the match between the size of capsules and sand pores. The capsules are likely to be deformed to fit in the pores of sand, without being crushed or becoming part of the load bearing skeleton of sand.

The released percent of tung oil increases with an increase in the capsule content in the case of mixing but exhibits an inverse relationship with capsule content during compaction. During the mixing process, the capsules ruptured due to the interaction with the mixing tools rather than the sand particles. Consequently, a higher capsule content increases the interactions with the mixing tool, leading to an elevated percentage of capsule breakage and cargo release. On the contrary, during the compaction process, capsules are primarily ruptured by the sand particles. Increased capsule content can promote interaction between the capsules rather than the sand particles. Owing to their lower stiffness, an assumption is that the capsules may experience reduced breakage or leakage when coming into contact with other capsules, resulting in a reduced percentage of tung oil release.

3.3 Maximum and minimum dry density

The maximum and minimum dry density of sand and sand-capsules mixtures were tested (Sect. 2.5) and shown in Table 2. With an increasing percentage of capsules, the maximum and minimum dry density of the sand-capsules mixture decreased. As the capsules content increased from 0 to 4%, 8%, and 12%, the minimum dry density of sand-capsules mixtures decreased from 1.29 to 1.21, 1.14, and 1.13 kg/m^3. The maximum dry density of sand-capsules mixtures decreased from 1.56 to 1.53, 1.48, and 1.46 kg/m^3, respectively. As the density of capsules were smaller than silica sand, with a greater percentage of additions, the density of the sand-capsules mixture decreased. However, the density reduction may not correlate with an increase in the volume of the voids. Note that density was calculated based on bulk and volume measurements of the system sand-capsules. Since the capsules are softer than sand, it is expected that they may fill or be squeezed into the pores.

3.4 Shear strength of sand-capsules mixtures

3.4.1 Shear strength of sand-capsules mixtures with fresh tung oil

The shear strength responses of the sand and sand-capsules mixtures at different normal stresses are presented in Fig. 7. Figure 7a shows the horizontal displacement versus the stress ratio (τ/σ). The shear strength behavior of the sand and the samples with 4% capsules follow a strain-softing response, while with the increase in the capsules content, the samples with 8% and 12% capsules showed the strain strain-hardening trend. A lower stiffness of the sand-capsules mixtures also explains such behavior [30]. Young's modulus of blank calcium alginate is reported to be in the range of 0.5–5.0 N/mm^2 [16]. With the increase in the capsules content in the sand, a greater number of interactions between the sand grains and capsules were expected. The interaction with the low-stiffness particles of capsules leads to a strain-hardening response [22].

The deformation of sand-capsules mixtures is shown in Fig. 7b, c. Figure 7b plots the vertical displacement versus the horizontal displacement, showing the dilation process. The shear displacement of sand-capsules mixtures with higher capsules content had lower vertical displacement during shear. For example, the vertical displacement at the end-of-shearing of 4% capsules was 0.98 mm, with increasing of capsules content to 8% and 12%, the vertical displacement decreased to 0.56 mm and − 0.04 mm. Figure 7c shows the dilatancy ($\delta\upsilon/\delta h$) versus the horizontal displacement. The deformation of the sand-capsules mixtures shows a dilation decrease with increasing capsules content, which could be explained by a greater compression of capsules due to a higher capsules content inside the mixture. Furthermore, the released tung oil also contributes to a lower dilatancy of sand samples during shearing due to lubrication at the inter-particle's contacts.

Figure 8a, b shows the fitting of normal stress and shear stress at the peak state and end-of-shearing. Note that not all samples achieved the critical state. For the interest of

accuracy and consistency, stress values are selected for a horizontal displacement of 8 mm and referred to in the paper as 'end-of-shearing'. The value of peak friction angle and end-of-shearing friction angle of sand and sand-capsules mixture was determined and summarized in Table 3. With the increasing of capsules content, the friction angle at peak state φ_{max} decreased. The friction angle at peak state of sand samples was 42.7° while the friction angle at peak state of sand samples mixed with 4%, 8%, and 12% capsules decreased to 41.9°, 35.8°, and 34.7° respectively.

The stress-dilatancy relationship of sand and sand samples mixed with 4%, 8%, and 12% capsules are shown in Fig. 8e. The general form of stress-dilatancy relationship can be expressed as:

$$\phi_{\mathrm{d}} = \varsigma \cdot \psi + \phi_{\mathrm{es}} \tag{5}$$

where ϕ_d = mobilized friction angle, ψ = dilation angle, ς = dilatancy coefficient, and ϕ_{es} = end-of-shearing friction angle [12]. A larger dilatancy coefficient ς indicates lower interparticle friction [12]. In this experiment, by increasing the capsules content, the dilatancy coefficient ς (obtained from the trendlines) of sand mixed with capsules was significantly larger than that of sand, increasing from 0.67 (sand) to 1 (4% capsules), 2.02 (8% capsules) and 1.81 (12% capsules), indicating the lower interparticle friction of sand-capsules mixtures. Furthermore, with the increase of capsules content, the end-of-shearing friction angle decreased.

The addition of capsules with fresh tung oil had a negative effect on sand mechanical strength, as exemplified by the decrease of friction angle (either at peak state or end-of-shearing). On the other hand, the addition of capsules contributed to the decrease in sand volumetric strains during shearing. However, this effect was amplified with the increase of capsules content from 4 to 8% and 12%. The capsules content of 4% proved an acceptable capsules addition, by only decreasing the peak friction angle of sand by 3.8% and contributed to the decrease of volumetric strain.

3.4.2 Volumetric response of capsules breakage and compression

The volumetric response due to capsules breakage and compression was calculated and shown in Fig. 9. The clean sand exhibits dilation primarily attributed to particle movement, given the inherent high stiffness of sand. By contrast, when the sand is mixed with soft capsules, the dilation encompasses both particle movement and capsules breakage and compression. With the increase of capsule content in soil, the volumetric response associated with both capsules breakage and compression increased. Specifically, the vertical displacement from capsules breakage and compression was 0.49 mm, 0.86 mm, and 1.5 mm for capsules content of 4%, 8%, and 12%, respectively. Capsules' breakage and compression contributed to a reduction in the overall dilation observed in the sand-capsule mixtures.

3.4.3 Impact of sample bulk density, relative density, and void ratio

To evaluate the influence of sample bulk density, relative density, and void ratio, a control test was conducted, as depicted in Fig. 10. When the void ratio and relative density were kept consistent with the sand containing 4% capsules, it was observed that the peak strength remained nearly unchanged. The addition of capsules had a notable effect on the reduction in volumetric dilation, as shown in Fig. 10b, cWhen the bulk density was the same as that of the sand-capsules mixture, the shear strength was found to be 18.5 kPa, which was lower than that of the sand-capsules (31.5 kPa). In addition, compared to the sand-capsules mixture, the sand sample with the same bulk density displayed a reduced dilation behavior. This disparity can be attributed to the capsules having a lower specific gravity of 0.96 compared to the sands (i.e., 2.65). When the bulk density of the sand was controlled to be the same as that of the sand-capsules mixture, the resulting void ratio was larger. In this case, the void ratio reached 0.90, in contrast to 0.78 for the sand-capsules mixture.

3.4.4 Release of fresh tung oil during shear

This section refers to the release of fresh tung oil during shearing. Figure 11a shows the content of tung oil in sand and Fig. 11b shows the released cargo percentage of capsules. After shearing, approximately 40% of cargo released out from capsules with the tung oil content in sand in the range of 1–3%. The capsules breakage and cargo release amount were affected by the extent of horizontal displacement, vertical stress, and capsules content in the sand. A greater amount of cargo released in the shear zone (subjected to greater horizontal strains) rather than the

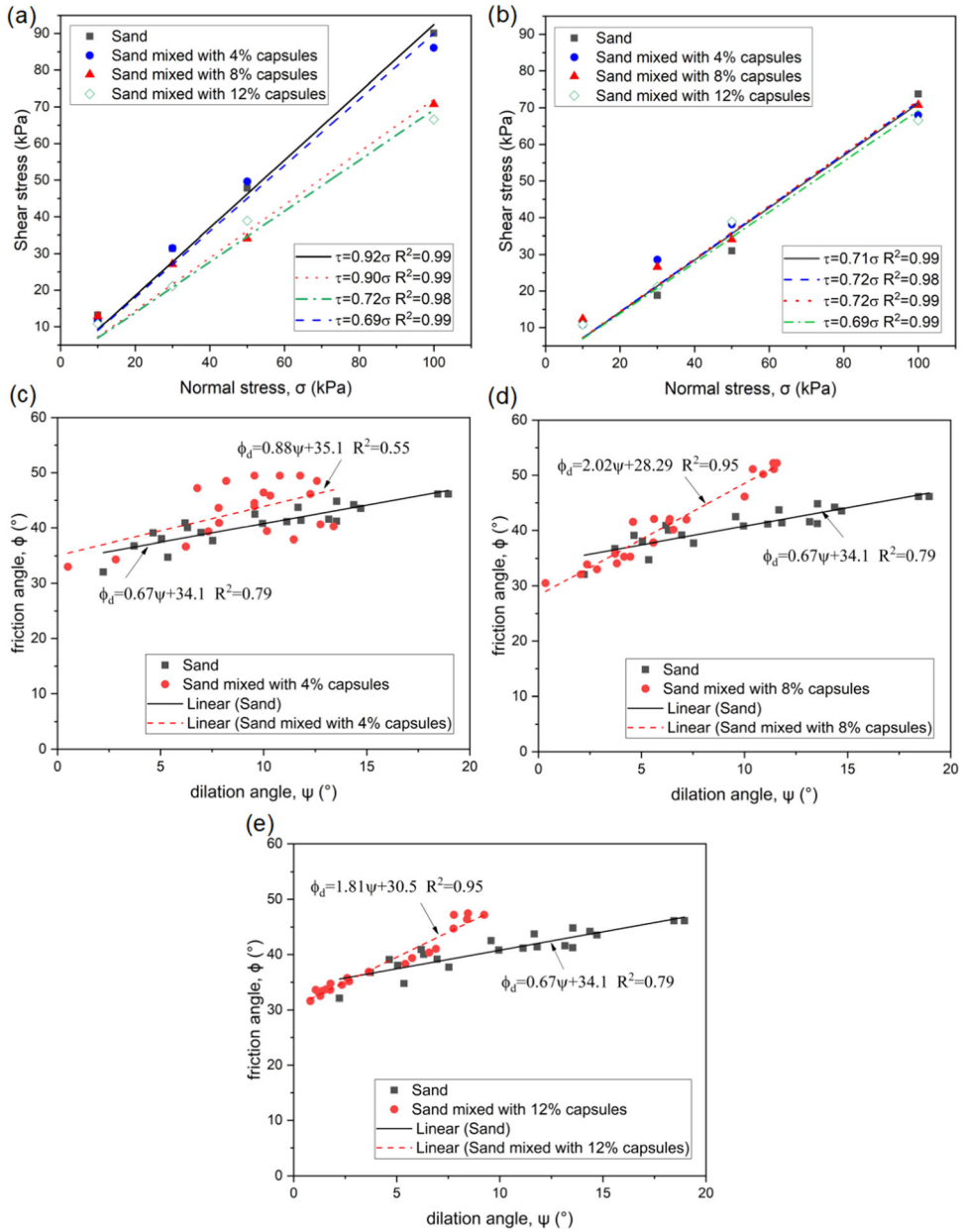

Fig. 8 Fitting of the direct shear test data of silica sand mixed with tung oil-calcium alginate capsules. Shear stress-normal stress fittings at: **a** peak state; **b** near-constant-volume state. Stress–dilatancy relationships of: **c** 4% capsules content; **d** 8% capsules content; **e** 12% capsules content

particles above and below and where the sand is subjected to vertical compression mostly (limited vertical strains). For example, the tung oil content in the compression areas is 0.9%, while the content of tung oil in the shear zone is 2.1% (8% capsules, 30 kPa vertical stress). A combination of greater horizontal strains and volumetric changes in the shear zone explains a greater breakage of capsules and release of cargo. With the increase of vertical stress, the content of tung oil in the sand and released cargo percentage increased. For example, the content of tung oil in the sand shear zone was 1.7%, 2.1%, 2.48%, and 2.4% for the vertical stress of 10 kPa, 30 kPa, 50 kPa, and 100 kPa (8% capsules content). With the increase of capsules content, the content of tung oil in the sand increased, but the

Table 3 Friction angles at peak state and end-of-shearing of sand, sand mixed with 4% capsules, 8% capsules, and 12% capsules with fresh Tung oil (φ = friction angle; $_{max}$ = peak state; $_{es}$ = end-of-shearing)

Parameter	Sand	Sand-4% capsules mixture	Sand-8% capsules mixture	Sand-12% capsules mixture
φ_{max} /°	42.7	41.9	35.8	34.7
φ_{es} /°	35.4	35.6	35.7	34.7

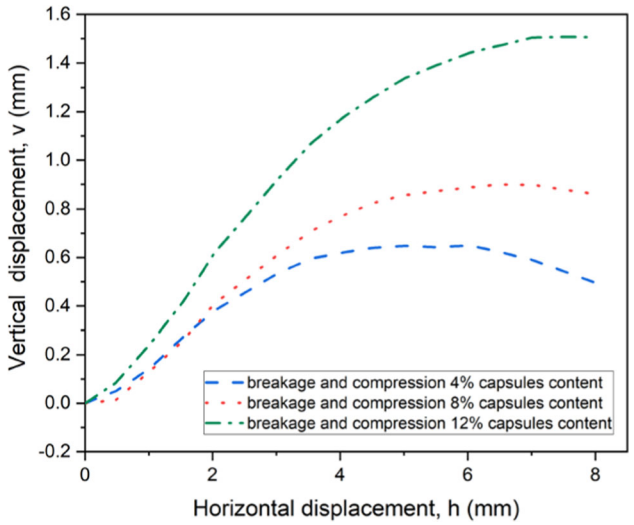

Fig. 9 Volumetric response from particle movement and capsules breakage and compression. (vertical stress of 30 kPa, capsules content of 4%, 8%, and 12%)

released cargo percentage remained nearly unchanged. For example, for a capsule's content increase from 4 to 8% and 12%, the content of tung oil in the sand shear zone increased from 0.79 to 1%, 2.38%, and 3.02% (at 50 kPa vertical stress). However, the released cargo percentage of capsules did not increase, remaining at 34.7%, 42.6%, and 36%. As mentioned, the release of cargo was controlled by the capsules multi-chamber structure and extent of horizontal strains, which is not related to the capsules content in the sand. As a result, the released cargo from single capsules did not change while the increase of capsules number lead to higher cargo content in the sand. The SEM images of ruptured tung oil-calcium alginate capsules after shearing are shown in Fig. 12.

3.5 Recovery of sand shear strength by polymeric capsules with aged tung oil

The recovery of sand mechanical performance by aged tung oil-calcium alginate capsules was corroborated. The aged tung oil refers to the tung oil that has been released from the capsules and undergone hardening. Figure 13 shows the shear strength behavior of sand, sand with blank-alginate capsules, and sand with tung oil-calcium alginate capsules at a relative density of 70%. As mentioned in Sect. 2.7, the sand-capsules mixtures were initially sheared to break and release Tung oil, placed in a controlled environment for the tung oil hardening and formation of a sand-tung oil composite, and re-sheared to assess the shear strength recovery. As shown in Fig. 13a, throughout the second shear stages, the shear strength of the clean sand decreased. With the introduction of capsules, there was an increase in shear strength compared to the clean sand. The extent of shear strength recovery achieved through the introduction of capsules was quantified with comparison to the shear strength of clean sand in the second shearing stage. The sand strength recovery with tung oil capsules was related to the normal stress applied, with the stress ratio reducing with increasing normal stress: 2.15, 1.49, 1.11, and 0.86 for normal stress of 10, 30, 50, and 100 kPa, respectively. By contrast, the peak stress ratio of sand without capsules were 1.24, 1.03, 0.94, and 0.88 (for normal stress of 10, 30, 50, and 100 kPa). The sand shear strength recovery had a 73%, 45%, and 18% increase for normal stress of 10, 30, and 50 kPa. For normal stress of 100 kPa, the stress ratio at the peak state decreased by 2%. It suggested that although the blank capsules had a negative effect on the sand strength, the tung oil cargo was able to overcome such effect and recover the sand shear strength.

Figure 13b, c shows the deformation of sand, sand-blank alginate capsules and sand tung oil-calcium alginate capsules. The addition of blank capsules decreased sand dilation. The vertical displacement of recovered sand was 1.13 mm, 1.14 mm, 1.11 mm, and 0.61 mm (for normal stress of 10, 30, 50, and 100 kPa), which was larger than the sand mixed with blank alginate capsules, ranging from 0.78 to 0.23 mm. While blank capsules decreased sand dilation, the hardened Tung oil lightly cemented sand particles, leading to a dilation increase.

The friction angle and cohesion of recovered sand at peak state and end-of-shearing is shown in Fig. 14 and Table 4. Sand-blank alginate capsules had a lower friction angle comparing to clean sand, decreasing from 39.3° to

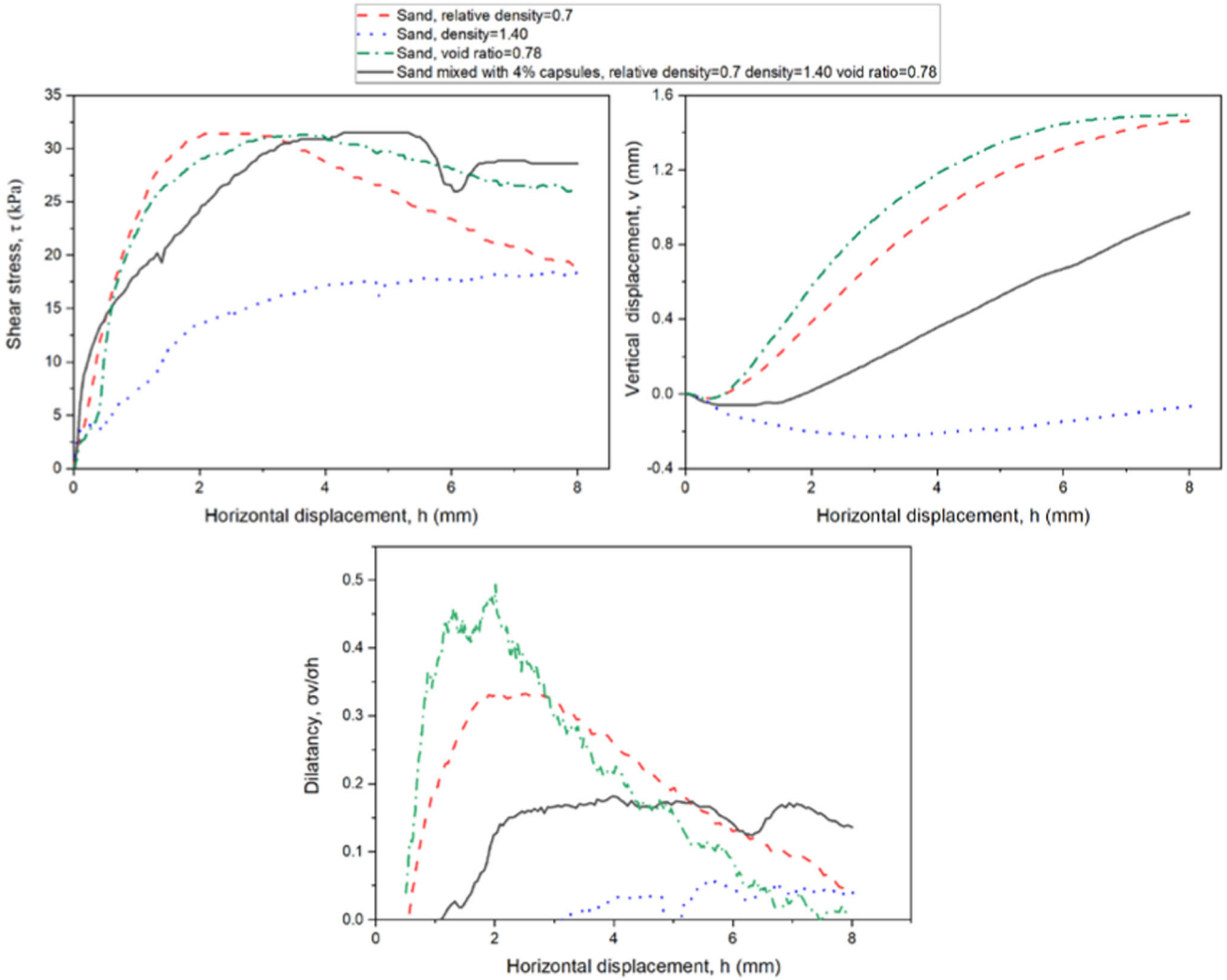

Fig. 10 The shear responses of the sand and sand mixed with tung oil-calcium alginate capsules prepared under the same bulk density, relative density, and void ratio, tested a normal stress of 30 kPa: **a** shear stress (τ) versus horizontal displacement (h); **b** vertical displacement (v) versus horizontal displacement (h); **c** dilatancy ($\delta v/\delta h$) versus horizontal displacement (h)

34.6° (peak state), and from 36.4° to 34.8° (end-of-shearing), respectively. For sand-tung oil alginate capsules with hardened tung oil, the friction angles decreased, from 34.5° to 30.7° for peak state and end-of-shearing state, respectively. However, for sand-tung oil alginate capsules, the cohesion at peak state significantly increased after recovery, from 6.9 to 18.6 kPa. The released tung oil from capsules hardened while being oxidated, bonding sand particles, and enhancing sand cohesion (Fig. 15). The reduction in soil friction angle and increase in cohesion explain the greater strength recovery observed under lower normal stresses. Specifically, when the normal stress is lower, the influence of cohesion on the soil strength becomes more pronounced. For the control group (clean sand), which were also sheared multiple times, the shear strength decreased with subsequent shearing event. The benefit of the capsules becomes evident in their ability to counteract this reduction in shear strength by facilitating cohesion and improving particle bonding.

3.6 Limitations and future work

Given that the current study investigated the feasibility of capsules-based soil strength recovery, future research should encompass a broader range of influential factors, including capsule type, various cargos, soil-to-capsule size ratios, and soil moisture content, among other factors. The hardening process of tung oil relies on the exposure to air,

which poses limitations in fully saturated conditions. Future research ought to develop methods and cargo-shell systems that can facilitate ground improvement in saturated conditions.

These findings indicate that the utilization of tung oil-calcium alginate capsules is most suitable for shallow soil depths (3 m given a dry density of 1.6 g/cm^3) characterized by relatively low normal stresses (< 50 kPa), where enhanced cohesion plays a pivotal role in augmenting shear strength.

4 Conclusions

This study demonstrates that it is feasible to encapsulate a healing agent (tung oil) into calcium alginate capsules and recover the shear strength of sands. The main conclusions of this research are detailed next. (1) Tung oil-calcium alginate capsules have a high survivability (> 90%) during mixing and compaction. (2) The addition of capsules reduced the maximum and minimum dry density of the sand. (3) The tung oil alginate capsules effect on the sand mechanical properties, prior to hardening, i.e. with liquid tung oil, depends on the capsules content. When the content of capsules is equal to or less than 4%, its effect on the

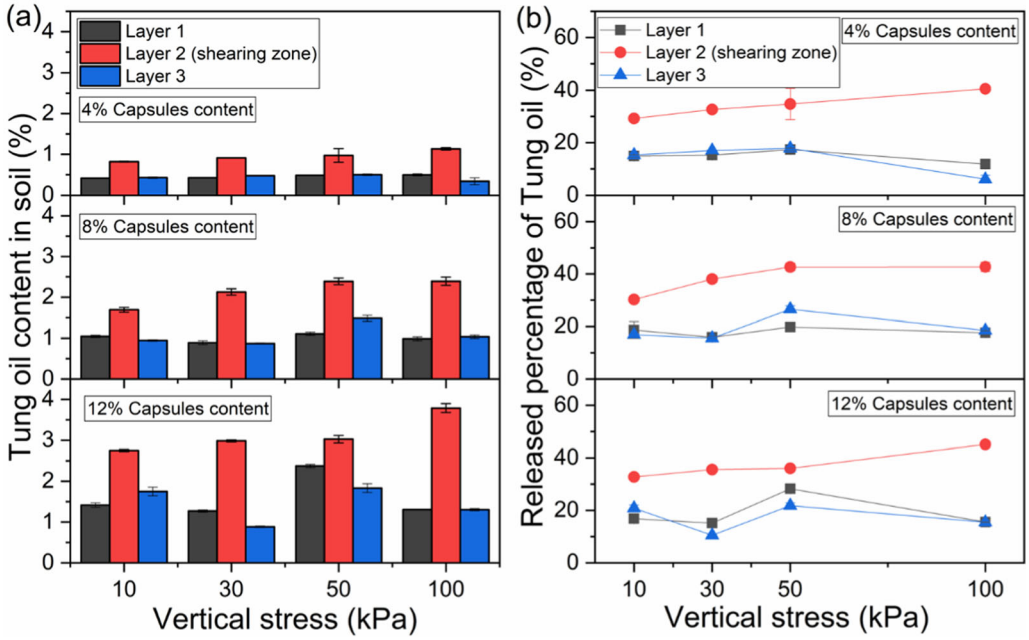

Fig. 11 Tung oil release during shear of silica sand mixed with tung oil-calcium alginate capsules. **a** Released tung oil content in sand; **b** released tung oil percentage

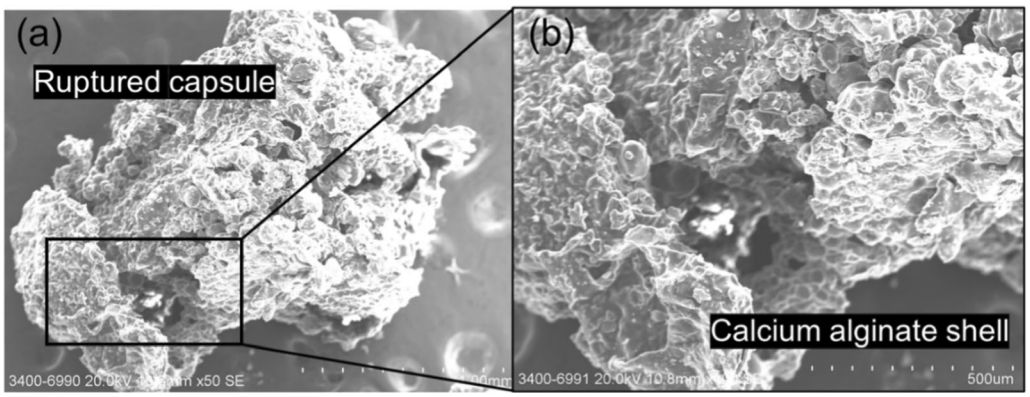

Fig. 12 SEM photomicrographs of ruptured tung oil-calcium alginate capsules after shearing

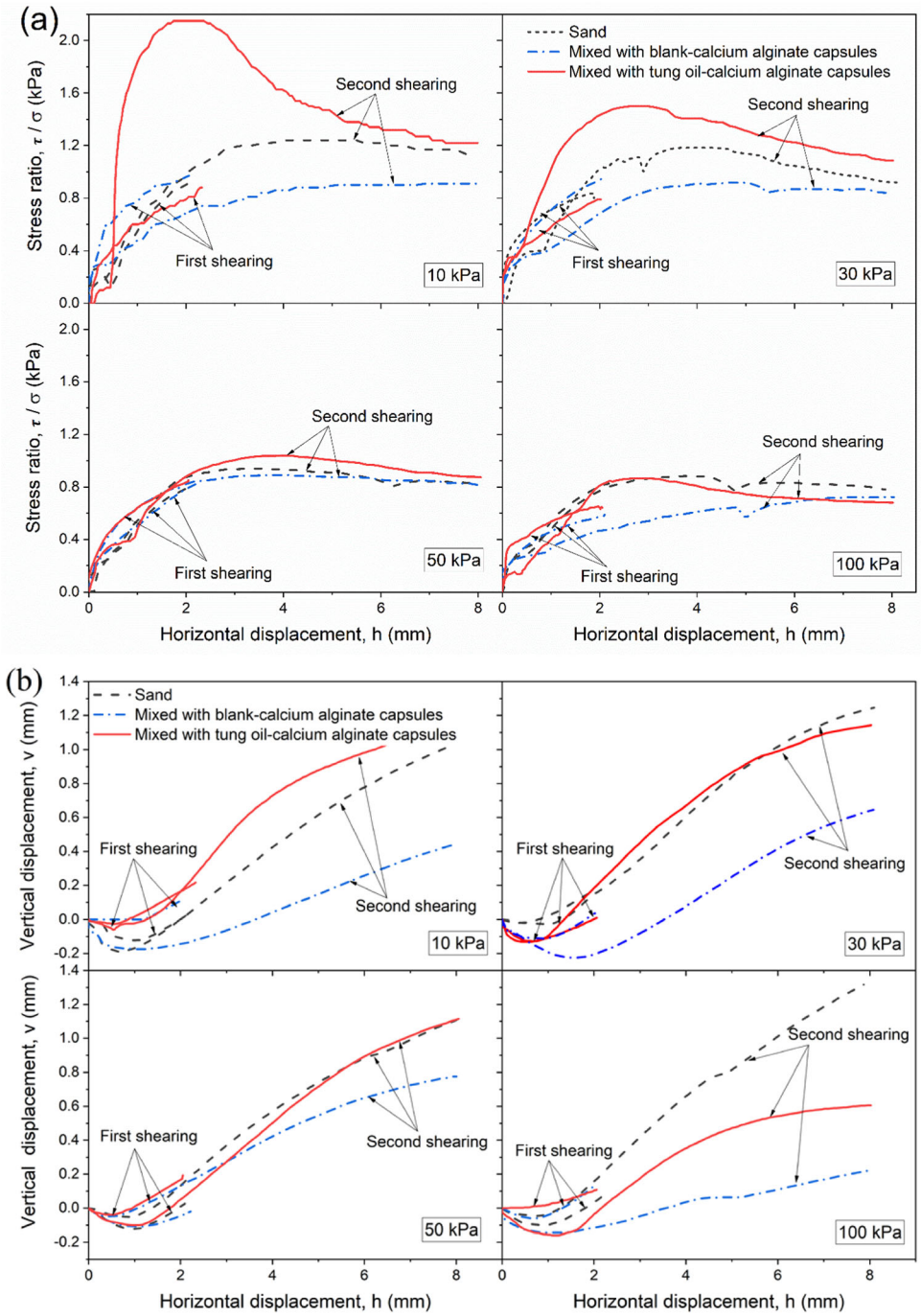

Fig. 13 The shear response of sand, sand mixed with blank-calcium alginate capsules, and sand mixed with 4% tung oil-calcium alginate capsules under normal stress of 10 kPa, 30 kPa, 50 kPa, and 100 kPa. Samples were sheared in two stages: first shearing to allow the release of fresh tung oil, followed by hardening, and second shearing of the hardened sand-tung oil composite. **a** stress ratio (τ/σ) versus horizontal displacement (h); **b** vertical displacement (v) versus horizontal displacement (h); **c** dilatancy ($\delta v/\delta h$) versus horizontal displacement (h)

shear strength of the sand is relatively small. For a capsule's content greater than 4%, the sand shear strength decreased markedly. With the increase of the content of capsules, the shear stress at peak state and end-of-shearing also decreases. (4) Sand particles movement lead to the breakage of capsules and cargo release. In the shear zone, approximately 60% of tung oil is released out of capsules. (5) Tung oil-calcium alginate capsules recover the sand shear strength after pre-shearing and hardening of tung oil. The mixtures increased by 73%, 45%, and 18% at 10 kPa,

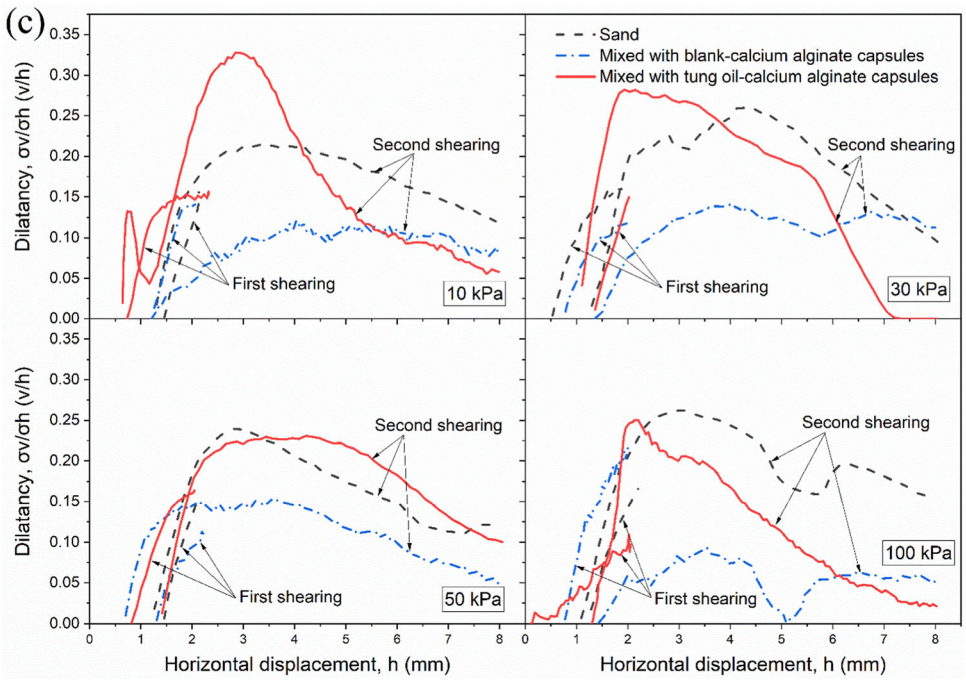

Fig. 13 continued

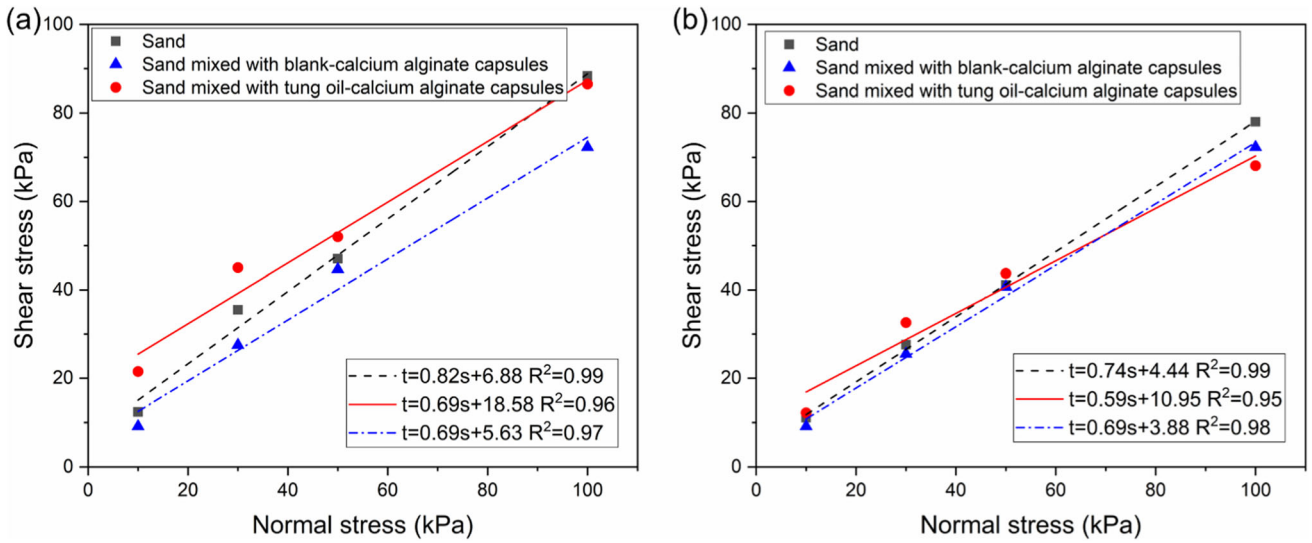

Fig. 14 Recovered shear stress-normal stress fitting of sand, sand mixed with blank-calcium alginate capsules, and sand mixed with tung oil-calcium alginate capsules: **a** peak state; **b** end-of-shearing

Table 4 Friction angle and cohesion at peak state and end-of-shearing of sand, sand mixed with 4% capsules with aged tung oil (TAC) and sand mixed with blank capsules (BAC) (φ = friction angle; c = cohesion; $_{max}$ = peak state; $_{es}$ = end-of-shearing)

Parameter	Sand	Sand TAC mixture	Sand BAC mixture
$\varphi_{max}/^{\circ}$	39.3 ± 3.0	34.5 ± 4.3	34.6 ± 3.8
c_{max}/kPa	6.9 ± 3.0	18.6 ± 4.4	5.6 ± 3.8
$\varphi_{es}/^{\circ}$	36.4 ± 0.8	30.7 ± 4.3	34.8 ± 1.8
c_{es}/kPa	4.4 ± 0.8	10.9 ± 4.4	3.9 ± 1.8

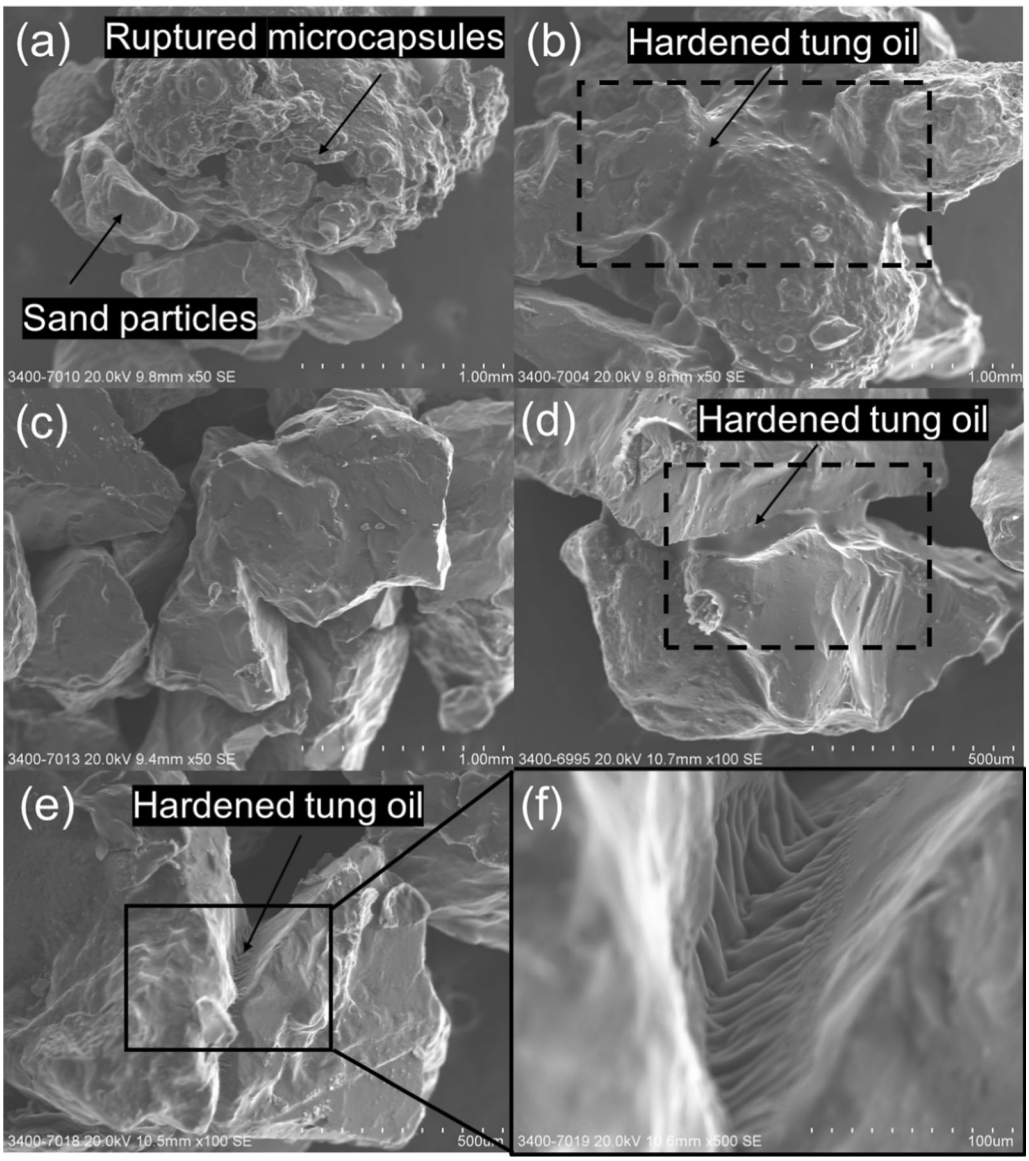

Fig. 15 SEM photomicrographs of sand particles bonded by released and hardened tung oil from capsules

30 kPa, and 50 kPa, respectively. The recovery mechanism relies on the release and hardening of tung oil cargo due to oxidation, bonding of sand particles and enhanced sand cohesion. These findings indicate that the utilization of tung oil-calcium alginate capsules is most suitable for shallow soil depths characterized by relatively low normal stresses, where enhanced cohesion plays a pivotal role in augmenting shear strength. In the field, capsules could be delivered by pre-mixing with the soil followed by compaction. Despite the preliminary nature of this study, the interaction of microcapsules with soil particles under shear and the resulting shear strength recovery suggests its potential in diverse soil engineering scenarios, including, for instance, the potential to arrest landslide initiation, control differential settlement or reduce ground movements near excavations.

Acknowledgements This work was supported by a Collaborative Research Fund from the Research Grants Council (HK) (C6006-20GF), seed funding grant from The University of Hong Kong (201910159115), Royal Society International Exchanges 2020 R3 (IES\R3\203024).

Data availability The datasets generated during and/or analysed during the current study are available from the corresponding author on reasonable request.

References

1. Al-Mansoori T, Norambuena-Contreras J, Micaelo R, Garcia A (2018) Self-healing of asphalt mastic by the action of polymeric capsules containing rejuvenators. Constr Build Mater 161:330–339
2. ASTM, D (2006) Standard test methods for minimum index density and unit weight of soils and calculation of relative density. In: West Conshohocken PA
3. Augst AD, Kong HJ, Mooney DJ (2006) Alginate hydrogels as biomaterials. Macromol Biosci 6(8):623–633
4. Bekas D, Tsirka K, Baltzis D, Paipetis AS (2016) Self-healing materials: a review of advances in materials, evaluation, characterization and monitoring techniques. Compos B Eng 87:92–119
5. Bolton M (1986) The strength and dilatancy of sands. Géotechnique 36(1):65–78
6. Botusharova S, Gardner D, Harbottle M (2020) Augmenting microbially induced carbonate precipitation of soil with the capability to self-heal. J Geotech Geoenviron Eng 146(4):04020010
7. Cao B, Souza L, Xu J, Mao W, Wang F, Al-Tabbaa A (2021) Soil mix cutoff wall materials with microcapsule-based self-healing grout. J Geotech Geoenviron Eng 147(11):04021124
8. Carey TJ, Stone N, Kutter BL (2020) Grain size analysis and maximum and minimum dry density testing of Ottawa F-65 sand for LEAP-UCD-2017. Model tests and numerical simulations of liquefaction and lateral spreading. Springer, Cham, pp 31–44
9. Chan L, Lee H, Heng P (2002) Production of alginate microspheres by internal gelation using an emulsification method. Int J Pharm 242(1–2):259–262
10. Chen K, Qi R, Xing X, Sufian A, Lourenço SDN (2023) Constriction size retention criterion for calcium alginate microcapsules in granular materials. Powder Technol 413:118034. https://doi.org/10.1016/j.powtec.2022.118034
11. Chow TT, Long H, Mok H, Li K (2011) Estimation of soil temperature profile in Hong Kong from climatic variables. Energy Build 43(12):3568–3575
12. Dai BB, Yang J, Zhou CY (2016) Observed effects of interparticle friction and particle size on shear behavior of granular materials. Int J Geomech 16(1):04015011
13. De Muynck W, De Belie N, Verstraete W (2010) Microbial carbonate precipitation in construction materials: a review. Ecol Eng 36(2):118–136
14. Dry CM, Corsaw MJT (1998) A time-release technique for corrosion prevention. Cement Concr Res 28(8):1133–1140. https://doi.org/10.1016/S0008-8846(98)00087-8
15. Giannaros P, Kanellopoulos A, Al-Tabbaa A (2016) Sealing of cracks in cement using microencapsulated sodium silicate. Smart Mater Struct 25(8):084005
16. Gombotz WR, Wee SF (2012) Protein release from alginate matrices. Adv Drug Deliv Rev 64:194–205
17. Grant GT, Morris ER, Rees DA, Smith PJC, Thom D (1973) Biological interactions between polysaccharides and divalent cations: the egg-box model. FEBS Lett 32(1):195–198. https://doi.org/10.1016/0014-5793(73)80770-7
18. He Z, Qian J, Qu L, Yan N, Yi S (2019) Effects of Tung oil treatment on wood hygroscopicity, dimensional stability and thermostability. Ind Crops Prod 140:111647. https://doi.org/10.1016/j.indcrop.2019.111647
19. Ju Y-H, Sari N, Go A, Wang M-J, Agapay R, Ayucitra A (2020) Preparation of epoxidized fatty acid ethyl ester from tung oil as a bio-lubricant base-stock. Waste Biomass Valoriz 11:4145–4155. https://doi.org/10.1007/s12649-019-00749-z
20. Kaklamani G, Cheneler D, Grover LM, Adams MJ, Bowen J (2014) Mechanical properties of alginate hydrogels manufactured using external gelation. J Mech Behav Biomed Mater 36:135–142. https://doi.org/10.1016/j.jmbbm.2014.04.013
21. Kanellopoulos A, Giannaros P, Al-Tabbaa A (2016) The effect of varying volume fraction of microcapsules on fresh, mechanical and self-healing properties of mortars. Constr Build Mater 122:577–593. https://doi.org/10.1016/j.conbuildmat.2016.06.119
22. Kim H-K, Santamarina JC (2008) Sand–rubber mixtures (large rubber chips). Can Geotech J 45(10):1457–1466
23. Ko FWY, Lo FLC (2018) From landslide susceptibility to landslide frequency: A territory-wide study in Hong Kong. Eng Geol 242:12–22. https://doi.org/10.1016/j.enggeo.2018.05.001
24. Lin H, Lourenço SDN, Yao T, Zhou Z, Yeung AT, Hallett PD, Paton GI, Shih K, Hau BCH, Cheuk J (2019) Imparting water repellency in completely decomposed granite with Tung oil. J Clean Prod 230:1316–1328. https://doi.org/10.1016/j.jclepro.2019.05.032

25. Lin H, Weitz HJ, Paton GI, Hallett PD, Hau BC, Lourenço SD (2022) Ecotoxicity assessment of hydrophobized soils. Environ Geotech 40:1–8
26. Morris ER, Rees DA, Thom D, Boyd J (1978) Chiroptical and stoichiometric evidence of a specific, primary dimerisation process in alginate gelation. Carbohyd Res 66(1):145–154
27. Orive G, Hernández RM, Gascón AR, Pedraz JL (2006) Encapsulation of cells in alginate gels. In immobilization of enzymes and cells. Springer, Cham, pp 345–355
28. Pathak TS, Yun J-H, Lee J, Paeng K-J (2010) Effect of calcium ion (cross-linker) concentration on porosity, surface morphology and thermal behavior of calcium alginates prepared from algae (Undaria pinnatifida). Carbohydr Polym 81(3):633–639. https://doi.org/10.1016/j.carbpol.2010.03.025
29. Rees DA, Welsh EJ (1977) Secondary and tertiary structure of polysaccharides in solutions and gels. Angew Chem, Int Ed Engl 16(4):214–224
30. Rouhanifar S, Afrazi M, Fakhimi A, Yazdani M (2020) Strength and deformation behaviour of sand- rubber mixture. Int J Geotech Eng 15(9):1078–1092. https://doi.org/10.1080/19386362.2020.1812193
31. Rowe PW (1962) The stress-dilatancy relation for static equilibrium of an assembly of particles in contact. Proc Royal Soc London Ser A Math Phys Sci 269(1339):500–527
32. Samadzadeh M, Boura SH, Peikari M, Ashrafi A, Kasiriha M (2011) Tung oil: an autonomous repairing agent for self-healing epoxy coatings. Prog Org Coat 70(4):383–387. https://doi.org/10.1016/j.porgcoat.2010.08.017
33. Schonemann A, Edwards HG (2011) Raman and FTIR microspectroscopic study of the alteration of Chinese tung oil and related drying oils during ageing. Anal Bioanal Chem 400(4):1173–1180. https://doi.org/10.1007/s00216-011-4855-0
34. Shields Y, De Belie N, Jefferson A, Van Tittelboom K (2021) A review of vascular networks for self-healing applications. Smart Mater Struct 30(6):063001
35. Tang Y, Xu J (2021) Application of microbial precipitation in self-healing concrete: A review on the protection strategies for bacteria. Constr Build Mater 306:124950
36. Terzis, D, Laloui L, Dornberger S, Harran R (2020) A full-scale application of slope stabilization via calcite bio-mineralization followed by long-term GIS surveillance. Geo-Congress 2020: Biogeotechnics
37. Testing A. S. f., & Materials (2000) Standard test methods for laboratory compaction characteristics of soil using standard effort. In: ASTM International West Conshohocken, PA, USA
38. Wan P, Liu Q, Wu S, Zhao Z, Chen S, Zou Y, Rao W, Yu X (2021) A novel microwave induced oil release pattern of calcium alginate/nano-Fe3O4 composite capsules for asphalt self-healing. J Clean Prod 297:126721. https://doi.org/10.1016/j.jclepro.2021.126721
39. Xu S, García A, Su J, Liu Q, Tabaković A, Schlangen E (2018) Self-healing asphalt review: from idea to practice. Adv Mater Interfaces 5(17):1800536
40. Žlahtič M, Mikac U, Serša I, Merela M, Humar M (2017) Distribution and penetration of tung oil in wood studied by magnetic resonance microscopy. Ind Crops Prod 96:149–157